Acta Neuropathol (2010) 119:235–248
DOI 10.1007/s00401-009-0586-0

ORIGINAL PAPER

Paclitaxel induces axonal microtubules polar reconfiguration and impaired organelle transport: implications for the pathogenesis of paclitaxel-induced polyneuropathy

Or A. Shemesh · Micha E. Spira

Received: 24 June 2009 / Revised: 18 August 2009 / Accepted: 18 August 2009 / Published online: 30 August 2009

Abstract In differentiated axons almost all microtubules (MTs) uniformly point their plus ends towards the axonal tip. The uniform polar pattern provides the structural substrate for efficient organelle transport along axons. It is generally believed that the mass and pattern of MTs polar orientation remain unchanged in differentiated neurons. Here we examined long-term effects of the MTs stabilizing reagent paclitaxel (taxol) over MTs polar orientation and organelle transport in cultured *Aplysia* neurons. Unexpectedly, we found that rather than stabilizing the MTs, paclitaxel leads to their massive polar reconfiguration, accompanied by impaired organelle transport. Washout of paclitaxel does not lead to recovery of the polar orientation indicating that the new pattern is self-maintained. Taken together the data suggest that MTs in differentiated neurons maintain the potential to be reconfigured. Such reconfiguration may serve physiological functions or lead to degeneration. In addition, our observations offer a novel mechanism that could account for the development of peripheral neuropathy in patients receiving paclitaxel as an antitumor drug.

Keywords Paclitaxel · Microtubules · Plus ends binding proteins · Axoplasmic transport · Peripheral neuropathy · *Aplysia*

Electronic supplementary material The online version of this article (doi:10.1007/s00401-009-0586-0) contains supplementary material, which is available to authorized users.

O. A. Shemesh · M. E. Spira (✉)
Department of Neurobiology, Institute of Life Science, The Hebrew University of Jerusalem, 91904 Jerusalem, Israel
e-mail: spira@cc.huji.ac.il

Introduction

In axons and dendrites of differentiated neurons, microtubules (MTs) form continuous arrays that extend from the cell body to the distal tips of the neurites. Whereas in axons almost all MTs uniformly point their plus ends anterogradely, towards the axonal tips, in dendrites approximately half of the MTs point their plus ends retrogradely towards the cell body, and the other half anterogradely [7, 15]. In both axons and dendrites, the MTs are not attached to the centrosome or to other structures, and the mechanisms that maintain their typical pattern of polar orientations are not known. It is generally believed that the mass and the typical pattern of MTs polar orientation remain unchanged in differentiated neurons. Nevertheless, under experimental conditions, the pattern of MTs polar orientations along the neurites may be significantly altered in support of regenerative processes [13, 14, 21, 53] or under conditions that lead to degeneration [49]. These findings indicate that the potential to reconfigure the MT polar pattern is preserved in differentiated neurons and challenges the belief that the polar orientation of MTs is maintained constant, under physiological conditions.

Of particular interest is to consider the consequences of subjecting neurons to pharmacological reagents that alter the MTs dynamics, as a side effect in cancer therapeutics. For example, the MT stabilizing drug paclitaxel (taxol) is extensively used as an anti-tumor drug [25]. 35–50% of cancer patients that receive paclitaxel develop peripheral neuropathy [1, 57]. Using rat as a model system, it was demonstrated that whereas paclitaxel does not lead to massive axonal degeneration [17] it causes partial terminal arbors degeneration of A- and C-fibers in the epidermis [50]. This is temporally associated with a significant increase in spontaneous firing of action potential by the

A- and C-fibers which presumably underlie the painful peripheral neuropathy [58]. Flatters and Bennet [17] and Xiao and Bennet [58] suggested that the paclitaxel-induced spontaneous firing is related to local depletion of energy resources due to paclitaxel-induced mitochondrial damage, and ensuing membrane depolarization. Since it was demonstrated that paclitaxel lead to impaired axoplasmic transport [38, 54], it is conceivable to assume that with time the excitable membrane properties of the neurites are altered leading to ectopic firing.

Here, we examined the hypothesis that as a side effect to the antitumor MTs-stabilizing functions, paclitaxel alters the dynamic properties of neuronal MTs leading to impaired organelle transport and peripheral neuropathy. Using confocal microscope imaging of the dynamic MTs plus ends and axoplasmic transport following days long exposure of cultured *Aplysia* neurons to low paclitaxel dosages (10–100 nM), we found that paclitaxel leads to reduction in the number of dynamic MTs and to reconfiguration of the dynamic MTs polar orientation, accompanied by impaired vesicles and mitochondrial transport.

The reported observations demonstrate that in contrast to the prevailing impression, the established pattern of dynamic MT polar orientations in differentiated neurons can be altered. Because of past difficulties to live-image the polar orientation of dynamic MTs, the possibility that MTs reorientation can take place and thereby alter the axoplasmic transport was not considered as a factor in promoting neurodegenerative diseases [11]. The present study demonstrates, at a basic level, that such mechanisms should be considered. Our observations offer a cell biological mechanism that could be considered to account for the development of peripheral neuropathy in humans undergoing antitumor treatment by paclitaxel.

Materials and methods

Cell culture

Neurons B1, B2 and bifurcated neurons from the buccal ganglia of *Aplysia* californica (*Aplysia* Resources Facility, Miami, FL, USA) were isolated and maintained in culture as described previously [33, 51]. In the present study, we refer to buccal neurons 1 and 2 collectively as B neurons.

Culture medium

The culture medium consisted of 10% filtered hemolymph, obtained from *Aplysia facciata* collected in the Mediterranean, diluted in modified Leibovitz's L 15 Medium as described previously [51].

Chemicals and pharmacological reagents

Paclitaxel (Sigma–Aldrich) was stored in a stock solution of DMSO at a concentration of 10 mM, diluted to a concentration of 10 μM in ASW and further diluted to a working concentration of 100 or 10 nM at the culture dish. DMSO concentration never exceeded 0.001% in the culture dish.

The fluid phase pinocytotic marker—sulforhodamine 101 (SR101, Kodak) was prepared as a stock solution of 10 mM in double distilled water and further diluted before use in artificial sea water (ASW) to a final concentration of 40 μM. Imaging of retrogradely transported pinocytotic vesicles labeled by SR101 was performed as described by Erez et al. [13].

Mitochondria were labeled by rhodamine B-[(phenanthren-9-yl)aminocarbonyl]bezyl ester (RPAC—a gift of Prof. Ioav Cabantchick, The Hebrew University). RPAC was prepared as a 3.84 mM stock solution in DMSO, and further diluted in the experimental dish to a final concentration of 0.5 μM [13, 49].

mRNA preparation and injection

mRNAs were transcribed in vitro using the recombinant transcription system, as described by our laboratory [45]. GFP-tagged EB3 [37, 52], was cloned in pCS2+ expression vector as previously described [45]. The transcribed mRNAs were pressure-injected into the cell body cytoplasm of cultured neurons 4–24 h after plating, as described [45].

Confocal microscope imaging

The systems used for confocal imaging included a Nikon C1 confocal system mounted on a Nikon TE-2000 Eclipse microscope system with a Nikon plan-Apo chromat 60× 1.4 NA oil objective. This system was equipped with three lasers: blue diode (405 nm), argon (488 nm) and green HeNe (543 nm). Images were collected and processed using EZ-C1 software at 20–24°C.

GFP-tagged proteins were excited at 488 nm; the emitted fluorescence was collected using a 515/30 nm filter. SR101 and RPAC were excited with the 543 nm laser, and the emission was collected through a 605/75 nm filter.

Color coding of SR101, RPAC or hOACTL-GFP of time-lapse sequences was achieved as follows: consecutive images within a time-lapse series were colored from blue to red. The individual images were then projected to produce a single image in which a moving organelle changes its color as a function of time. Immobile objects appear white reflecting the summation of the rainbow.

Image analysis

Images were analyzed offline using NIH ImageJ software (Bethesda, MD, USA) and MATLAB (MathWorks, Natick, MA, USA) and Laserpix (Media Cybernetics, L.P.). The figures were prepared using Photoshop (Adobe Systems) and FreeHand software (Macromedia, San Francisco, CA, USA).

Quantification of the EB3-GFP comet tail length, velocity and directionality

Quantification of single EB3-GFP comet tail length, velocity and directionality was done by image processing in MATLAB, which included the following main steps: (a) an area of interest (AOI) was defined. (b) Frames were converted into binary images, such that EB3 labeled fluorescent "comet tails" were separated from the background. (c) Comet tail length was assessed. (d) The directionality of a single "comet tail" was defined by comparing its position in two consecutive frames, providing a movement vector of individual comet tails. (e) An angle histogram of 100 comet tails within the AOI was produced. (f) Based on the image acquisition rate and the movement vector of each comet tail, EB3-GFP propagation velocity was calculated.

Weighed vector of EB3-GFP comets

To simplify the presentation of the polar orientation of an entire MT population within the main axon, we developed a quantitative parameter in the form of a weighted vector. The equivalent length of the weighted vector represents the overall polar orientations of the EB3-GFP comet tails within a standard AOI of 75 × 20 μm. To calculate the weighted vector, the propagation angle of 50 randomly selected comet tails from a standard AOI were determined. All 50 individual EB3-GFP comet tails were assigned an equal vector size of 1 (in arbitrary units-AU). The x and y components of the 50 vectors were extracted and a weighed vector whose size represents the overall movement of these EB3-GFP comet tails in the axon was calculated.

Quantification of transport of SR101 labeled organelles

In each standard AOI analyzed regarding its EB3 properties, 20 SR101-labeled organelles were selected randomly. The organelles were manually tracked along five frames using ImageJ (MTrackJ plugin) and trajectory data was extracted. Using inter-frame interval we calculated the velocity of each organelle. We defined a motile vesicle as a vesicle moving faster than 0.015 m/s since even stationary organelles can exhibit motion in a very small scale. We next calculated the percentage of organelles moving retrogradely out of motile organelles.

Statistical analysis

To determine the significance of alteration in the averages of EB3-GFP number length and velocity we used t-test. To compare sector distributions we used the Chi-square test.

Results

Characterization of the number, length, and propagation velocity of the EB3-GFP comet tails in control neurons

Cultured *Aplysia* neurons are characterized by the extension of a main neurite (referred to as axon) from the cell body and the elaborate branching of neurites from the axon's tip. The diameter of the axon is maintained constant in 90.48% of control neurons for over a week ($n = 21$, Fig. 1a).

As background information for the study of the long-term effects of paclitaxel over dynamic MTs and axoplasmic transport, we characterized the MTs dynamics along the main axons of cultured neurons for a period of 9 days. To that end we labeled the plus ends of dynamic MTs by intracellular microinjection of mRNA encoding the plus-end-tracking protein—EB3 (end binding protein 3) tagged by GFP [13, 14, 46, 49, 52]. EB3-GFP transiently binds to the polymerizing MTs plus ends. Thus, it moves with the growing MT's plus end tips forming a comet tail-like structure (Fig. 1b and Supporting Movie S1A). EB3 serves as a functional linker between the dynamic plus ends of MTs and the surrounding molecular nano-environment [23, 24, 29]. Thus, its use as a probe to track the MTs plus ends should be done with care not to alter the neurons physiology. In a number of studies from our laboratory we found that EB3-GFP expression in cultured *Aplysia* neurons does not affect the growth patterns, rates of neurites outgrowth, regeneration of the axon after axotomy, excitable membrane properties and synaptic transmission [13, 14, 46, 49, 52].

The physical features of EB3-GFP comet tails and other plus end binding proteins such as EB1, EB3 and CLIP-170 reflect some of the basic MTs characteristics [19, 23, 29]. The number of comet tails is proportional to the number of dynamically polymerizing MTs. The length of the comet tails strongly coincides with the rate of the microtubule growth or shortening [29, 39]. The translocation velocity of EB3-GFP comet tails reflects either the addition rate of tubulin dimmers to MTs plus ends [24, 28, 34], or/and the transport rate of short microtubules decorated by EB3-GFP along longer MTs [3, 12].

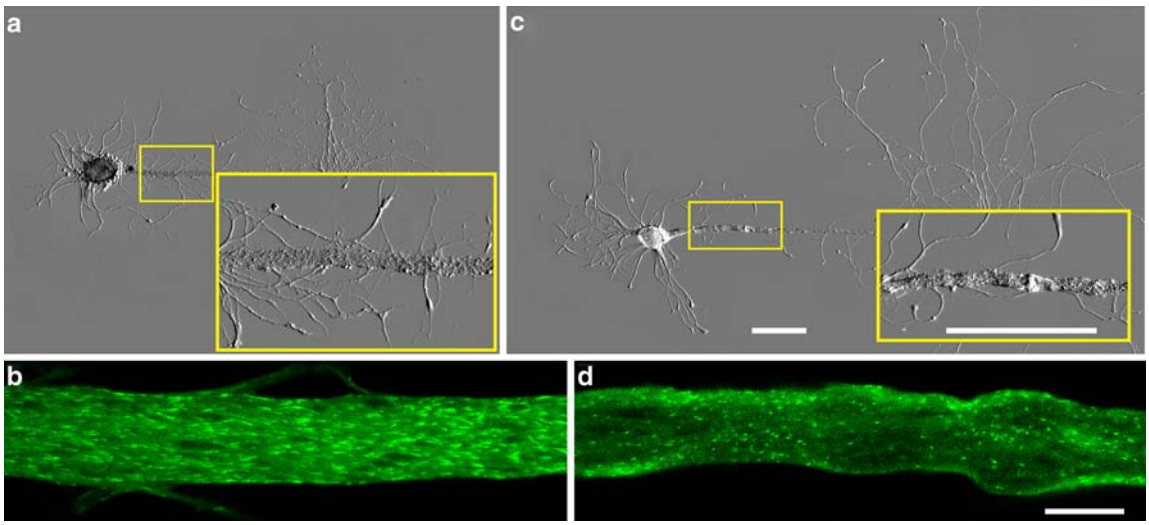

Fig. 1 Neuronal morphology and polar orientation of microtubules in a control neuron and a neuron bathed in 100 nM paclitaxel. **a** Typically the main axon of cultured B neuron maintains a constant diameter (The axonal segment within the *yellow rectangle* is enlarged -a, insert). **b** Visual examination of control neurons suggest that the majority of the EB3-GFP "comet tails" orient in parallel pointing the plus end anterogradely towards the tip of the axon (Supporting Movie S1A). **c** 24 h after microinjection EB3-GFP encoding mRNA, 100 nM paclitaxel was added to the culture medium. 72 h later the neuron revealed moderate swellings along the axon [the axonal segment indicated by the *yellow rectangle* in enlarged, insert (**c**)]. **d** Note that the EB3-GFP comet tails in the paclitaxel treated neuron are shorter than in the control (compare **d** to **b**), unevenly distributed and concentrate at the axons cortex. A substantial fraction of the EB3-GFP comet tails point in various angles in respect to the long axis of the axon (for quantitative analysis see Figs. 3, 4. Supporting Movie S1B). *Scale bars* 100 μm in **c** applies to **a**, 10 μm in **d** applies to **b**

Classical studies reported that whereas in axons the MTs point their plus end distally towards the tip of the axons, in dendrites approximately half of the MTs point the plus end in the opposite direction [4, 33]. Recently, it was recognized that in vertebrate axons approximately 18% of the MTs point the plus end retrogradely [34].

To characterize the directionality, number, length and propagation velocity of the EB3-GFP comet tails in cultured *Aplysia* neurons, we imaged neurons expressing EB3-GFP within a standard area of interest (AOI) of 75 μm × 20 μm in the main axon located 100–400 μm away from the cell body (Fig. 1a, c and Supporting Movie S1A). An example of the parameters collected from a single control neuron for up to 72 h after EB3-GFP mRNA microinjection is given in Fig. 2. Quantitative analysis of the above parameters measured from a population of neurons over time is detailed below.

Directionality of the MT plus ends in control neurons

Quantitative analysis of the MTs polar orientation performed on a group of five control neurons over a period of 7 days (Fig. 3a, b) revealed that the distribution of the MT polarity remained unchanged (see Statistical Appendix 1a). We analyzed 419, 401, 392 and 416 EB3-GFP comet tails 24 h, 72 h, 120 h and 7 days after EB3-GFP mRNA microinjection, respectively. In contrast to the prevailing view, which assumes that all MTs within axons point the plus end away from the cell body towards the tip of the axon [5], unbiased analysis readily revealed that approximately 30% of the MTs within the main neurite point their plus ends retrogradely and laterally rather than anterogradely (Fig. 3a). To simplify the presentation and discussion of the MTs polar orientations within an axon we subdivided the detailed angle histograms (Fig. 3a, b) to three categories as follows: (a) Anterograde direction—MTs that point their plus ends away from the cell body, within a section confined between 300° and 60°. (b) Retrograde direction—MTs that point their plus ends towards the cell body, within a section confined between 120° and 240°. (c) Lateral direction—microtubules that point their plus ends perpendicular to the anterograde or retrograde directions and are confined within 60 to 120° and 240 to 300° (Fig. 3a vertical lines and Fig. 3b). The unbiased analysis of control neurons revealed that the EB3-GFP labeled MTs are composed of a population in which 69.53% ± 1.97% of the plus ends point anterogradely, 14.23% ± 1.76% point retrogradely and 16.24 ± 0.77% point laterally. This distribution remained unchanged for over 7 days (see Statistical Appendix 1a).

Number of EB3-GFP comet tails in control neurons

The example depicted by Fig. 2 demonstrates that the number of EB3-GFP comet tails increases from the day

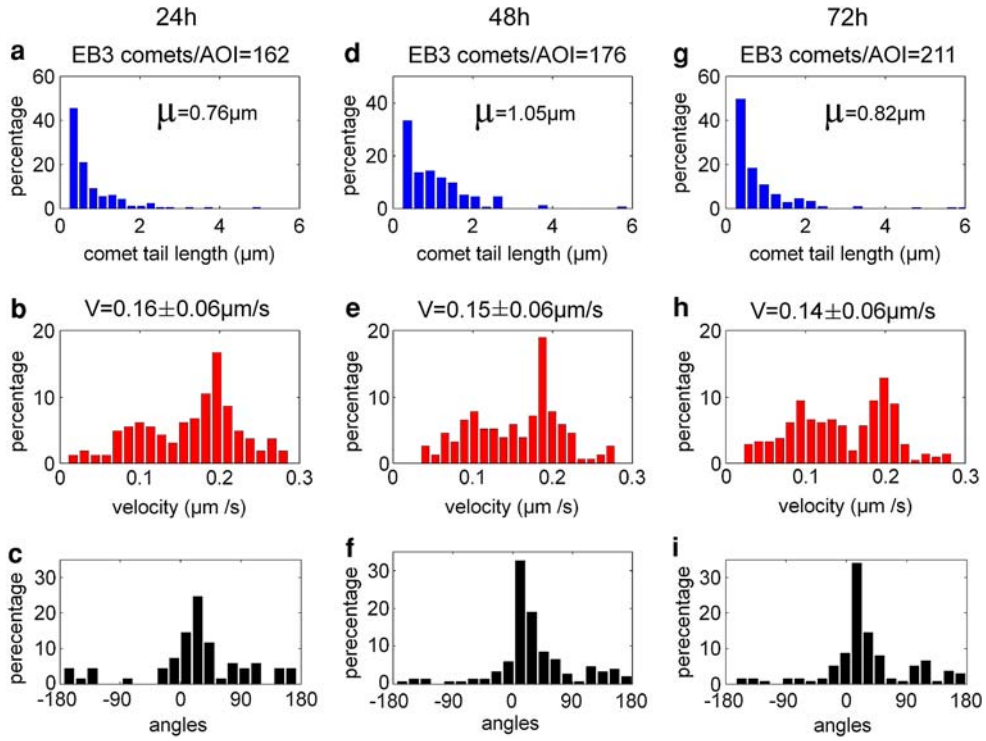

Fig. 2 Analysis of EB3-GFP "comet tails" features over time in a control neuron. A cultured neuron plated for 12 h was injected with EB3-GFP mRNA. The neuron was imaged 24 h (**a**–**c**), 48 h (**d**–**f**) and 72 h after injection (**h**–**i**). The number of EB3-GFP comet tails/standard AOI is given for each point in time. **a**, **d**, **g** EB3-GFP comet tails length was measured at different points in time. This revealed insignificant changes in the comet tails length (average length is given in each graph). **b**, **e**, **h** The propagation velocity of the EB3-GFP comet tails reveals two peaks, at 0.1 μm/s and at 0.2 μm/s. The average velocity of the comet tails propagation velocity is maintained constant over the observation period. **c**, **f**, **i** Directional vectors of the EB3-GFP comet tails reveal that the normal profile of MT polar orientations is maintained over the observation period

of EB3-GFP mRNA injection, until 72 h post injection and remains statistically unchanged for the next days. In a quantitative analysis based on five neurons, the number of EB3-GFP comet tails increased by 12.75%, 24–72 h post EB3-GFP mRNA microinjection, from 169.4 ± 10.6 at 24 h ($n = 5$) to 191 ± 13.3 ($n = 5$) at 72 h. This increase was found to be statistically significant using *t*-test ($n = 5$; two-tailed; alpha = 0.05; $p = 0.0368$). Thereafter, the average number of comet tails was 178.13 ± 17.39 and 187.40 ± 28 on the 5th and 7th days after injection (correspondingly). These further changes were insignificant relative to each other (*t*-test; 72 h against 120 h; $n = 5$; two-tailed; alpha = 0.05; $p = 0.3504$; 120 h against 7 days; $n = 5$; two-tailed; alpha = 0.05; $p = 0.5415$). In summary, the number of EB3-GFP comet tails initially increases and reaches a steady state 3 days after the mRNA injection. We attribute the increase in the number of EB3-GFP comet tails to the time required for the neurons to translate, transport and reach a steady state concentration of the exogenous EB3-GFP probe.

EB3-GFP comet tails length in control neurons

The histogram of EB3-GFP comet tail lengths in control neurons fits an exponential distribution with a mean—μ of 0.86 ± 0.06 μm on the first day of observation (24 h after EB3-GFP mRNA microinjection), and 0.97 ± 0.05 μm 72 h following the microinjection (Fig. 2a, d, g). The increase in μ was not found significant using *t*-test ($n = 5$; two-tailed; alpha = 0.05; $p = 0.308$). 5 or 7 days later, the length of comets was 0.843 ± 0.02 μm and 0.854 ± 0.04 μm, respectively. At these points in time, the lengths did not significantly differ from initial observation (24–120 h; $n = 5$; two-tailed; alpha = 0.05; $p = 0.8585$, 24 h to 7 days; $n = 5$; two-tailed; alpha = 0.05; $p = 0.9794$).

Propagation velocity of EB3-GFP comet tails in control neurons

The propagation velocity of the EB3-GFP comet tails appeared to be bimodal, peaking at 0.1 and 0.2 μm/s. The average velocities did not change in any significant manner

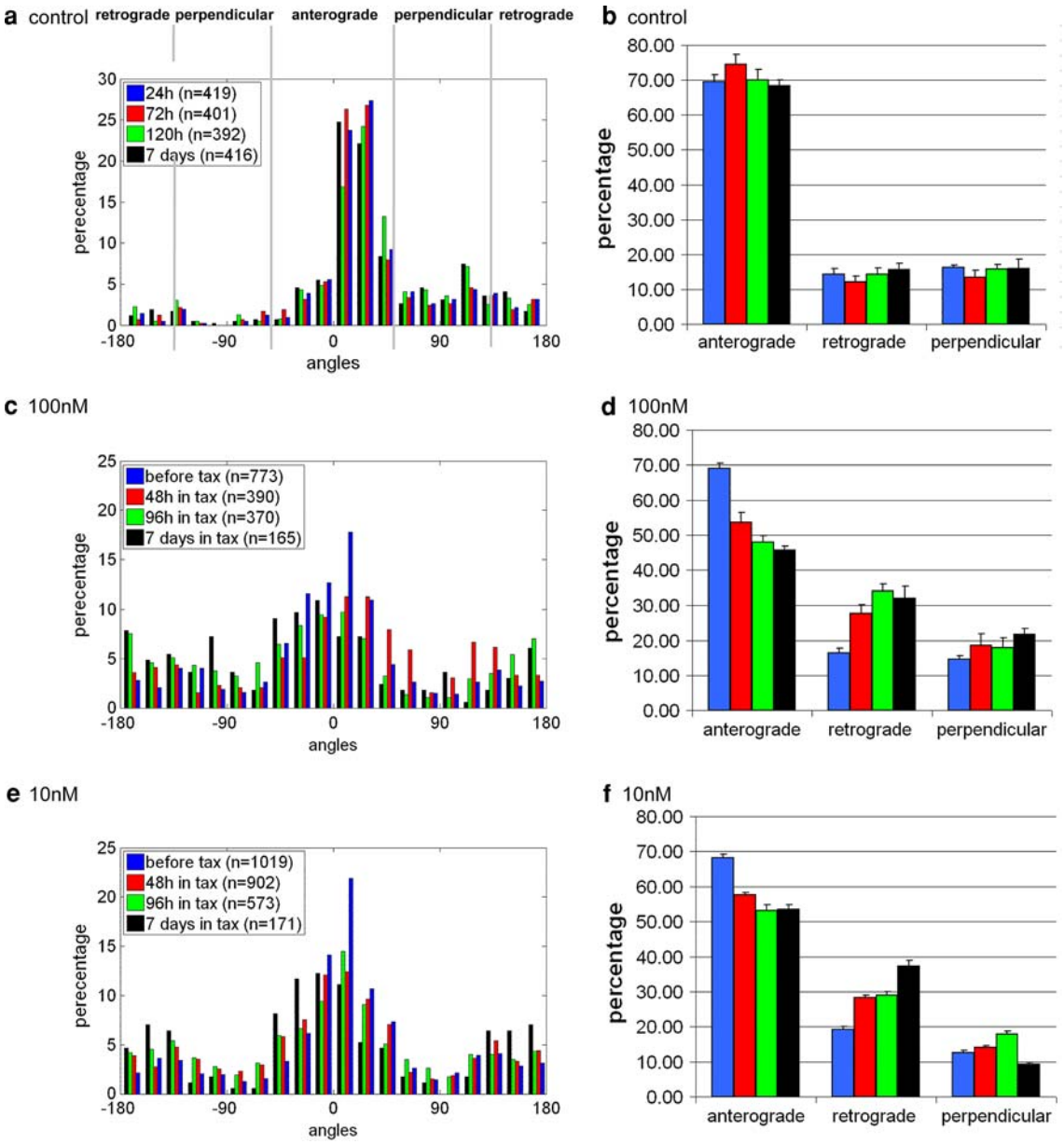

Fig. 3 Paclitaxel-induced alterations in the MTs polar orientation. Quantitative analysis of the EB3-GFP "comet tails" directional propagation in control neurons (**a**, **b**) and neurons exposed to 100 (**c**, **d**) or 10 nM (**e**, **f**) paclitaxel. The angles were measured in relation to the long axis of the axon (0°). **a**, **b** Control observations. 5 neurons were injected with EB3-GFP mRNA 12 h after plating. The neurons were imaged 24 h, 72 h, 120 h and 7 days after mRNA injection. The angles of all the EB3-GFP comet tails within the standard AOI are shown in the angle histogram (**a**). For the sake of convenience the angle histogram was subdivided to three sectors (*vertical lines* in **a**) anterograde, retrograde and perpendicular. The percentage of EGFP-EB3 comet tails pointing the plus end into each sector is shown in (**b**). **c** Five neurons were injected with EB3-GFP mRNA as described for (**a**) and imaged 24 h after the injection ("before tax"). Thereafter, these neurons were incubated in 100 nM paclitaxel, and angle histograms were produced for 48 h, 96 h and 7 days in paclitaxel ($n = 3$ for 7 days). The time points of observations are corresponding to those of control. The joint angle histogram of these results is shown in (**d**). **e** Seven neurons were injected with EB3-GFP mRNA and imaged one day later ("before tax"), and angle histograms were produced. Thereafter, these neurons were incubated in 10 nM paclitaxel, and joint angle histograms were produced for 48 h, 96 h and 7 days ($n = 3$ for 7 days). The joint angle histogram of these experiments is shown in (**f**)

over a period of 9 days in culture. At 24 h from EB3-GFP mRNA microinjection, it was 0.134 ± 0.0015 μm/s, at 72 h 0.138 ± 0.004 μm/s, on the 5th day 0.123 ± 0.002 μm/s and on the 7th day 0.128 ± 0.004 μm/s. The differences among these values were statistically insignificant (*t*-test; $n = 5$; two-tailed; alpha = 0.05; $p = 0.803$, 0.4795 and

0.7431). The bimodal distribution was maintained over time (Fig. 2b, e, h). The propagation velocity measured by us is within the range of propagation velocities of EB3-GFP comet tails reported for vertebrate axons [24, 28, 34, 52] and non-neuronal cells [39].

To conclude, in control neurons the number of EB3-GFP comet tails initially increases reaching a steady state level on day 3. Their length, propagation velocity and polar orientation remained unchanged for a duration of 7 days.

Effects of long-term incubation of neurons in paclitaxel

To characterize the effects of paclitaxel on the dynamic MT population within an axon, we exposed cultured neurons to 10 or 100 nM paclitaxel for up to 7 days. We noted that in the presence of 10 or 100 nM paclitaxel, 30.43% ($n = 23$) and 70%, ($n = 20$) of the neurons (correspondingly) developed swellings along the main axons within 1–3 days (Fig. 1b, d and Supporting Movie S1B). These neurons tended to detach from the substrate within 4–7 days. In contrast, in control experiments only a small fraction of the neurons (9.52%, $n = 21$) developed swellings 4 days after plating.

Reconfiguration of the microtubules polar orientations by paclitaxel

To study the effect of paclitaxel on MTs polar orientation, we analyzed two experimental groups of EB3-GFP expressing neurons using the methods detailed above. A group of 21 neurons were exposed to 100 nM paclitaxel and a group of 22 neurons were exposed to 10 nM paclitaxel. To reduce the variability, the control neurons ($n = 21$ as described above) were isolated from the same ganglia from which the neurons used for the paclitaxel experiments were isolated.

The experiments were conducted as follows: 12 h after culturing, EB3-GFP encoding mRNA was microinjected into the neurons. 24 h after plating we imaged the axons and collected the parameters for analysis as described above. Thereafter, paclitaxel was applied to the culture medium, and neurons were imaged once every 24 h for a total duration of 7–9 days.

We found (Fig. 3c, d and Supporting Movies S1 and S5) that within 48 h of 100 nM paclitaxel application, the percentage of MTs pointing their plus ends anterogradely was significantly reduced by 15.31% (from 69.00 ± 1.5% to 53.69. ± 2.81%, see Statistical Appendix 2a). This reduction was accompanied by a significant increase in the percentage of MTs that point the plus ends retrogradely from 16.39 ± 1.34% to 27.68 ± 2.53%, and a non-significant increase in the lateral sectors from 14.61% ± 1% to 18.63 ± 3.34% (see Statistical Appendix 2a). Following 96 h in 100 nM paclitaxel, the fraction of MTs that point the plus end anterogradely was 47.93 ± 1.81% significantly lower than the initial value (see Statistical Appendix 2a), but not changed in respect to the value obtained at 48 h (paired t-test; $n = 5$ AOIs; two-tailed; alpha = 0.05; $p = 0.2146$). We also observed a significant increase in the percentage of retrogradely pointing plus ends to 34.07% ± 1.97% and a non-significant change in the percentage of plus end MTs oriented laterally to 17.94 ± 2.78% (see Statistical Appendix 2a). Following 7 days of incubation in 100 nM paclitaxel, a further reduction in the percentage of MTs that point the plus end anterogradely was noticed to 45.64 ± 1.79%, significant change in the retrograde sector to 32.03% ± 4.06% and a non-significant increase in the perpendicular sectors to 22.33 ± 1.67% (see Statistical Appendix 2a).

In summary, 100 nM paclitaxel leads to significant alterations in the polar orientations of the dynamic MTs such that the percentage of MTs plus ends pointing anterogradely is reduced by approximately 23% along 7 days and the percentage of MTs that point in all other directions, especially retrogradely, is increased. These alterations have significant effects on the axoplasmic transport as described below.

To estimate the paclitaxel concentration which induces alterations in the MT polar orientation and MTs dynamics, we repeated the above observations using 10 nM paclitaxel (Fig. 3e, f and Supporting Movies S1 and S2). In summary, 10 nM paclitaxel exerts similar qualitative effects as 100 nM except that they develop at a slower rate and to a lesser extent (see Statistical Appendix 2a and 2b).

Paclitaxel induces a reduction in the number of EB3-GFP comet tails

Paclitaxel stabilizes both plus and minus ends of MTs [25]. Consistently we found that paclitaxel led to a decrease in the number of detectable EB3-GFP comet tails (Fig. 4). Whereas before paclitaxel application (24 h following EB3-GFP mRNA microinjection), 208.19 ± 14.4 comet tails were detected within the standard AOI, 48 h after the application of 100 nM paclitaxel, the number was reduced to 142 ± 16.33. This reduction (−35.4%) was found to be significant using t-test ($n = 5$; two-tailed; alpha = 0.05; $p = 0.039$). The number of comet tails did not change any further with values of 133.6 ± 31.10 comets 96 h later, and 117.33 ± 11.66 comets 7 days later.

In seven neurons incubated with 10 nM paclitaxel, we found a reduction in the average number of EB3-GFP comet tails from 160.43 ± 9.59 before paclitaxel incubation, to 115.71 ± 5.55, 109.86 ± 4.69 and 71 ± 8.66 following 48 h, 96 h and 7 days, respectively. The reduction in comet

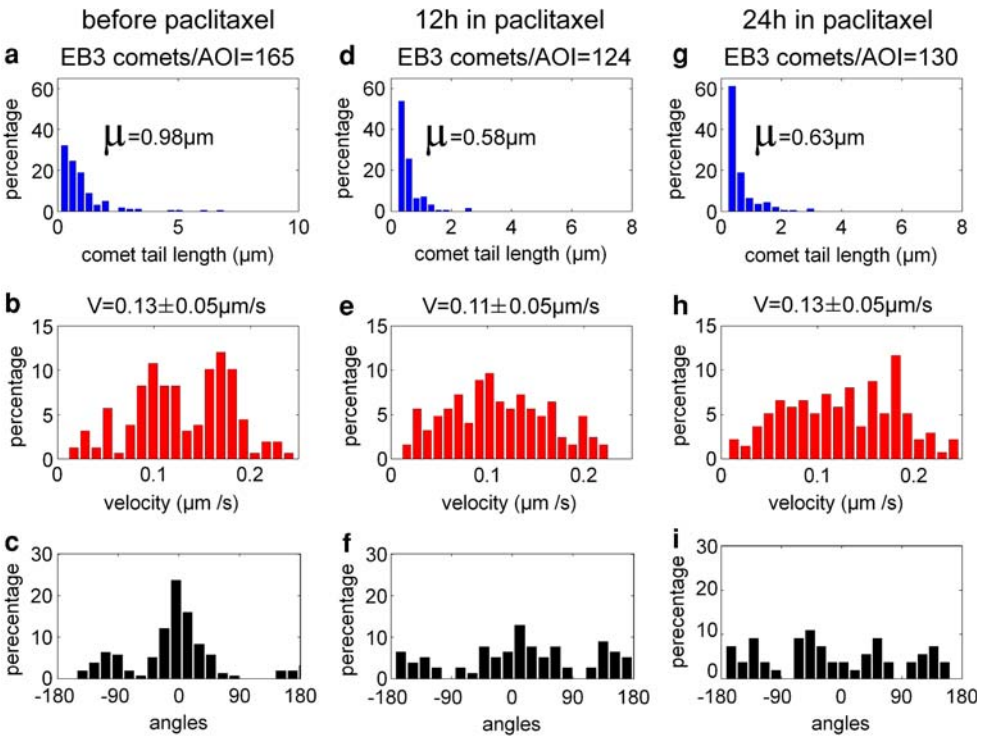

Fig. 4 Analysis of EB3-GFP features over time in a neuron exposed to paclitaxel. A cultured neuron injected with EB3-GFP mRNA was imaged during the first day following microinjection (**a**–**c**). Thereafter, the neuron was incubated in 100 nM paclitaxel and imaged 12 h (**d**–**f**) and 24 h post EB3-GFP mRNA injections (**h**–**j**). The number and length of the EB3-GFP comet tails decreased with time (**a**, **d** and **g**, average length is given in each graph), while the average propagation velocities of the comet tails remained unchanged (**b**, **e** and **h**). With time, the polar distribution of the MTs plus end was altered (**c**, **f** and **i**)

tail number in the first 48 h was found significant (*t*-test; $n = 7$; two-tailed; alpha = 0.05; $p = 0.024$).

Paclitaxel induces shortening of the EB3-GFP comet tails

As early as 2 h after 100 nM paclitaxel application, shortening of EB3 comet tails was observed. Following 48 h of 100 nM paclitaxel incubation, a 15.6% reduction in EB3-GFP length from 0.81 ± 0.04 μm to 0.68 ± 0.025 μm was detected (Fig. 4). This shortening was found significant using *t*-test ($n = 5$; two-tailed; alpha = 0.05; $p = 0.0118$). 96 h and 7 days following application of paclitaxel, the comet tail length was 0.69 ± 0.04 μm and 0.63 ± 0.05 μm, respectively. This further shortening was not found significant (48 h to 96 h, $n = 5$; two-tailed; alpha = 0.05; $p = 0.785$, 96 h to 7 days, $n = 5$; two-tailed; alpha = 0.05; $p = 0.3205$). In neurons incubated with 10 nM paclitaxel, a significant shortening of 35.98% was noticed in the first 48 h from 0.87 ± 0.01 μm to 0.64 ± 0.01 μm ($n = 7$; two-tailed; alpha = 0.01; $p = 0.0016$). 96 h and 7 days following paclitaxel incubation, the comet tails length was of 0.59 ± 0.01 μm and 0.64 ± 0.01 μm, respectively. These changes were not significant relative to each other (48 h to 96 h; $n = 7$; two-tailed; alpha = 0.05; $p = 0.186$, 96 h to 7 days; $n = 3$; two-tailed; alpha = 0.05; $p = 0.2449$). These results indicate that comet tail length shortened in paclitaxel within the first 48 h and then remained stable.

Paclitaxel does not change the EB3-GFP comet tails translocation velocity

Measurement of the translocation velocity of individual EB3-GFP comet tails indicated that the bimodal velocity distribution of the untreated neurons changed following paclitaxel application such that the two peaks (0.1 and 0.2 μm/s) could not be detected (Fig. 4). Nevertheless, the average velocity before paclitaxel incubation significantly differed from the average velocity 48 h after application of 100 nM (0.13 ± 0.003 μm/s and 0.11 ± 0.007 μm/s respectively, *t*-test; $n = 5$; two-tailed; alpha = 0.05; $p = 0.0143$). The average velocity remained at 0.11 for 7 days. In neurons incubated with 10 nM paclitaxel, the average velocity remained constant at 0.12 μm/s for 7 days ($n = 7$).

Paclitaxel impairs organelle transport

To image retrograde transport, pinocytotic vesicles were labeled by the fluid phase pinocytotic marker—sulforhodamine 101 (SR101) as previously described by our laboratory [13, 49]. The labeled vesicles are transported retrogradely in a homogeneous manner along the entire cross section of the axon ($n = 5$, Fig. 5a, b and Supporting Movie S3). For the analysis we defined a motile organelle as a SR101 labeled fluorescent hotspot measuring 0.4–2.5 μm in size, which moves faster than 0.015 μm/s. According to this cutoff, 92.71 ± 3.61% of

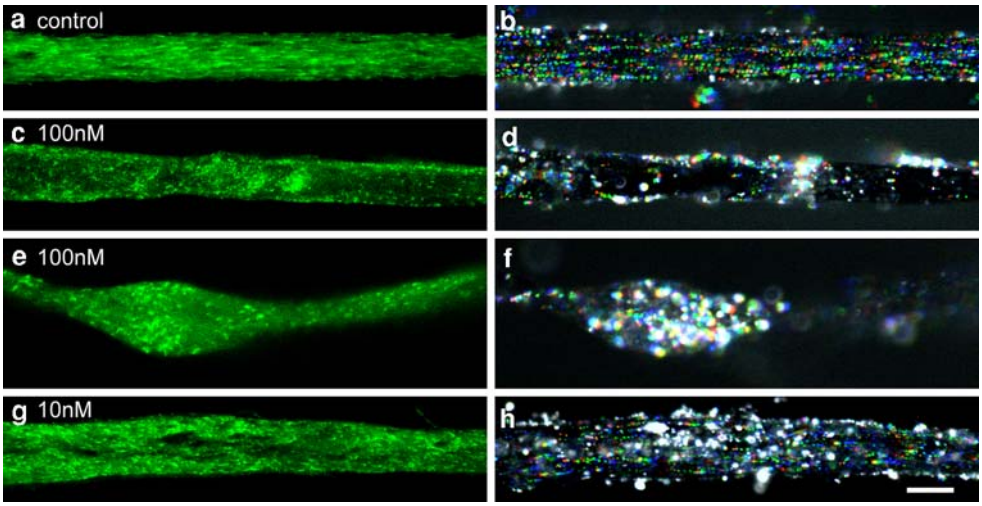

Fig. 5 Retrograde transport in control and paclitaxel treated neurons. A neuron was microinjected with EB3-GFP mRNA and imaged 72 h later, demonstrating normal MTs polar orientations. **b** Retrograde transport of the fluid phase pinocytotic marker SR101 was imaged every 4.5 s (see Supporting Movie S3). The first ten frames were color coded and displayed as a single image. Note the linear retrograde transport (from *blue* to *red*) of SR101 labeled vesicles. *White spots* denotes stationary organelles. **c** A neuron expressing EB3-GFP for 24 h was exposed to paclitaxel for 48 h inducing MTs polar reorientations. **d** Color coding of the retrograde transport of SR101 labeled vesicles (10-frames taken 5.7 s apart) revealed that the number of transported vesicles is reduced and that a relatively large fraction of vesicles are not moving (see Supporting Movie S5). **e** A neuron expressing EB3-GFP for 24 h was exposed to 100 nM paclitaxel for 48 h revealed MT polar reorientation and axonal swelling. **f** Color coding of the retrograde transport of SR101 labeled vesicles (10-frames taken 5.7 s apart) revealed that the swollen compartment contains stationary organelles (see Supporting Movie S5). **g** A neuron expressing EB3-GFP for 24 h was incubated in paclitaxel for 48 h giving rise to reorientation of MTs polar orientations. **h** Color coding of the pinocytotic vesicles (10-frames taken 5.7 s apart) revealed that the retrograde transport is partially retarded (see Supporting Movie S4). *Scale bar* 10 μm

the SR101 labeled organelles in control neurons were dynamic. Of these motile organelles, 96.71 ± 1.35% were moving in a retrograde direction while the rest moved in the lateral and anterograde direction. In neurons exposed for 96 h to 10 nM paclitaxel ($n = 5$), a substantial fraction of the SR101 labeled organelles were stationary. We found that only 54.6 ± 10.21% were motile, and that 71.03% ± 14.67 out of the motile vesicles moved retrogradely (Fig. 5g, h and Supporting Movie S4). The percentage of motile organelles in control neurons and 10 nM paclitaxel treated neurons significantly differs. Within these populations, the percentage of retrogradely transported organelles is similar (see Statistical Appendix 3).

In neurons incubated for 48 h in 100 nM paclitaxel ($n = 6$), 40.44 ± 7.46% of SR101 labeled organelles were moving, while 72.96% ± 5.76% of dynamic vesicles were moving retrogradely (Fig. 5c, d, e, f and Supporting Movie S5). Both the percentage of motile organelles and the percentage of retrogradely transported organelles in control and 100 nM paclitaxel treated neurons significantly differ (see Statistical Appendix 3). The non-motile vesicles appeared to be trapped in aggregates between MTs that point their plus ends in different directions or where MTs were absent. This observation suggests that paclitaxel does not compete with molecular motors on MTs binding sites.

Transport of mitochondria was assessed using either RPAC [49] or the mitochondrial targeting sequence of human 3-oxoacyl-CoA thiolase (hOACTL) fused to GFP (hOACTL-GFP)[61]. In control neurons, bidirectional transport of elongated mitochondria is readily observed (Fig 6a, $n = 7$ for RPAC and $n = 2$ for hOACTL-GFP). Both in 10 nM paclitaxel ($n = 4$ and $n = 3$ for RPAC and hOACTL-GFP, respectively) and 100 nM paclitaxel ($n = 3$ and $n = 4$ for RPAC and hOACTL-GFP, respectively), transport of mitochondria was severely impaired (Fig 6b and c, Supporting movie S6). These observations implies that paclitaxel impairs the movement of mitochondria which is essential for many neuronal functions [43, 55].

Correlation between the loss of MTs polarity and impaired transport

The observations described above revealed that the relationship between the polar orientation of the MTs and transport directionality are not trivial. For example, whereas in control neurons approximately 70% of the MTs point their plus end anterogradely more than 90% of the SR101 labeled vesicles are transported retrogradely. To better establish the relationship between the polar orientation of the MT population and the directionality of

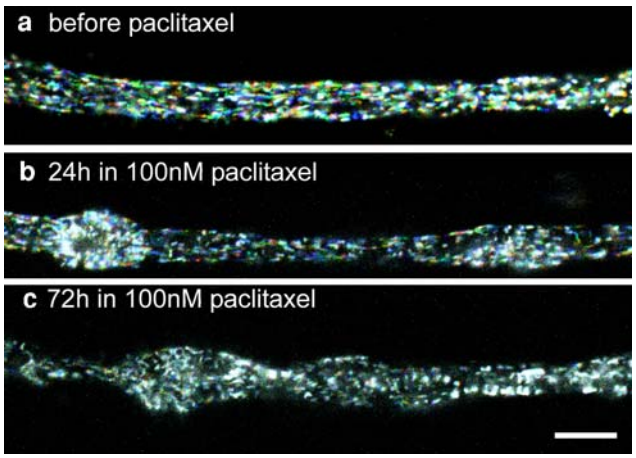

Fig. 6 Effect of paclitaxel over mitochondrial transport. **a** A buccal neuron was injected with hOACTL-GFP mRNA and imaged 24 h later. Ten frames of hOACTL-GFP labeled mitochondria were taken 5.3 s apart and color coded, so that each frame received a different color, from blue to red. Stationary mitochondria are color coded white. **b** Thereafter, the neuron was incubated in 100 nM paclitaxel and imaged 24 h later. Color coding as in (**a**). **c** The axon 72 h following paclitaxel incubation. Note that most hOACTL-GFP labeled organelles are stationary (*white* color coding). *Scale bar* 10 μm

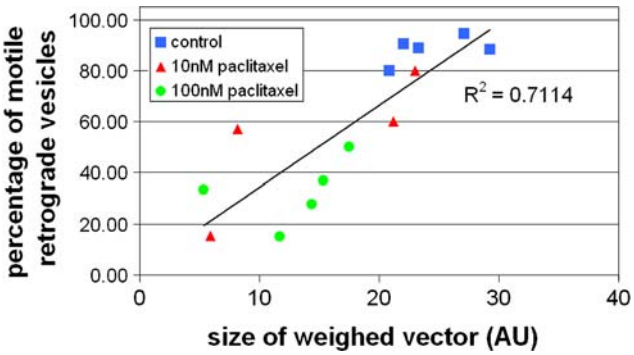

Fig. 7 Paclitaxel-induced loss of MTs polar orientation predicts impaired transport. The percentage of SR101 labeled vesicles which are both motile and retrogradely transported is plotted against the length of the equivalent directional vector of the MTs. This was done for 5 control neurons, four neurons incubated in 10 nM paclitaxel and five neurons incubated in 100 nM paclitaxel. Given in black is a linear regression line. A correlation coefficient of 0.71 was calculated indicating positive relations between the equivalent vector size and the percentage of the retrogradely transported SR101 labeled organelles

SR101 labeled organelles transport, we calculated an unifying equivalent directional vector that represents the directional propagation of the entire population of EB3-GFP labeled MTs (see Materials and methods). We found that in the five control neurons, the average length of the equivalent vectors was 33.23 ± 1.9 AU and 48 h later the vector length was 32.04 ± 2.22 AU. This −3.58% length change was insignificant (see Statistical Appendix 1b). In contrast, in neurons that were exposed to 10 nM ($n = 6$) and 100 nM ($n = 5$) paclitaxel, the weighted vectors significantly decreased within 48 h time, from 24.13 ± 0.98 AU to 14.51 ± 2.37 AU (−53.16%) and from 29.00 ± 1.37 AU to 14.89 ± 0.62 AU (−35.24%), respectively. These results indicate that the length of the equivalent vector remained unchanged over time in control neurons, however in paclitaxel-incubated neurons it was shortened in a time and concentration dependent manner (see Statistical Appendix 1b and 2b). Interestingly, we found that in control and paclitaxel-incubated neurons, a higher value of the equivalent vector length corresponded to a higher percentage of SR101-labeled organelles, which were both motile and retrogradely transported (Fig. 7). Taken together, these results point out that the size of equivalent vector, which is a measure of the polar orientation of the MT population is shortened by paclitaxel application, and that transport impairments are correlated with this shortening of weighed vector.

Paclitaxel induced MTs polar reorganization and impaired axoplasmic transport is not reversible

An imperative question is whether the paclitaxel-induced polar configuration of the MTs is reversible. This question is of interest because of two reasons. First, if the altered MT configuration recovers to control state upon wash it implies that the presence of a MT stabilizing reagent alters the equilibrium among the many proteins that stabilize the MTs and thereby maintain a new steady state. Alternatively, if the altered MTs polar orientation does not recover upon wash, then paclitaxel operates by shifting one steady state to a new one. Another aspect of this question is the reports that discontinuity of paclitaxel treatment in patients does not always abolish the neuropathic pain [6]. To address this question, we incubated four neurons in 100 nM paclitaxel for 48 h and documented polar reorientation of the MTs and impaired retrograde transport as described above (Fig. 8a, b). Thereafter, the culture medium containing paclitaxel was extensively washed away. 24–72 h following paclitaxel washout, we observed that the length of individual EB3-GFP comet tails and their number increased (Fig. 8h, k), indicating that the paclitaxel was effectively washed away. However, the MTs polar orientation and retrograde transport remained abnormal (Fig. 8c, d, j, m and Supporting movie S7). These results suggest that once the abnormal polar MT organization is established it does not revert to the normal template.

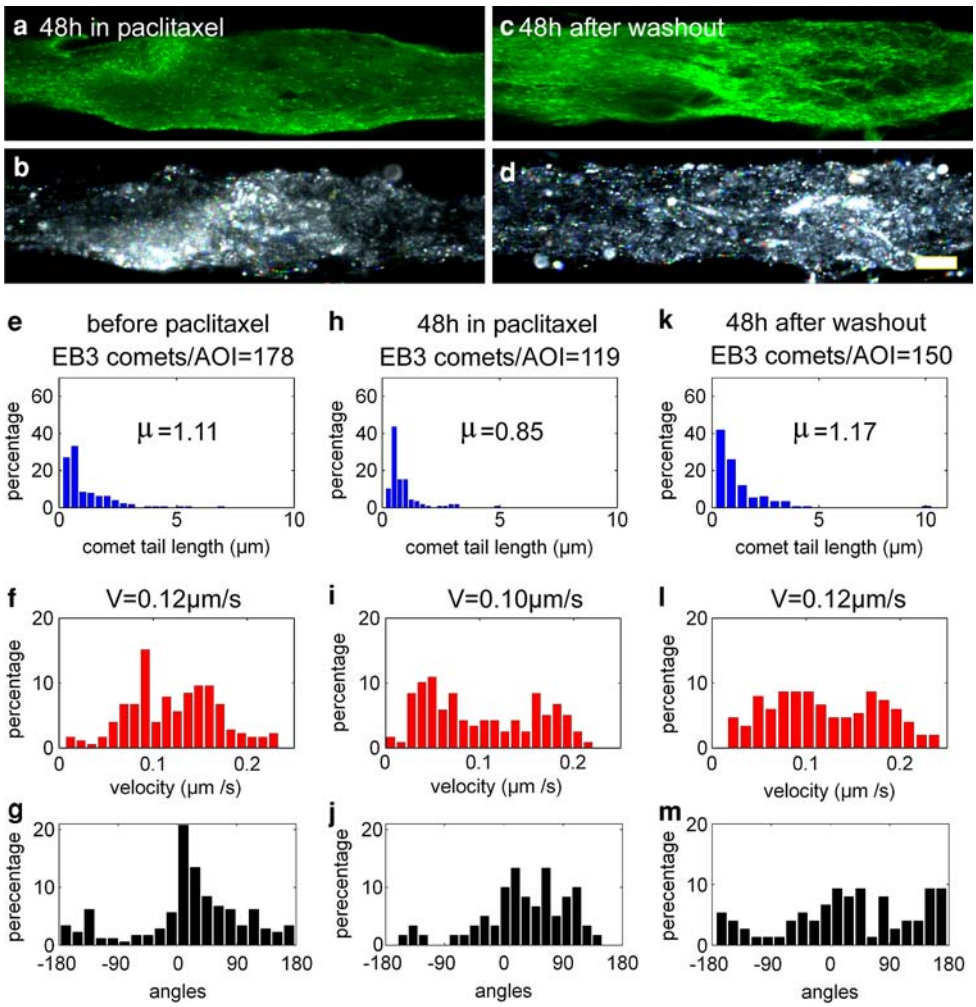

Fig. 8 Irreversibility of paclitaxel-induced alterations in MTs polar orientation. **a** A neuron was incubated in 100 nM paclitaxel for 48 h leading to alteration in the MTs polar orientation. **b** This was associated with impairments of the retrograde SR101 transport (color coding of 10-frames taken 5.7 s apart). Thereafter, paclitaxel was washed away from culture medium, and EB3-GFP (**c**) and SR101 (**d**) labeled vesicles were imaged 48 h later. The number and the length of the EB3 comet tails revealed partial recovery (**e**, **h** and **k** for before paclitaxel, 48 h in paclitaxel and 48 h after paclitaxel washout respectively). The velocity of the EB3-GFP comet tails did not change significantly (**f**, **i,** and **l** for before paclitaxel, 48 h in paclitaxel and 48 h after paclitaxel washout, respectively). The loss of MTs polar orientation did not recover following washout (**g**, **j**, and **m** for before paclitaxel, 48 h in paclitaxel and 48 h after paclitaxel washout, respectively)

Discussion

The results presented here imply that: (a) in contrast to the prevailing premise, the polar organization of the MTs in differentiated neurites can be altered. These observations raise the possibility that local and transient reconfiguration of the MTs polar orientation, under physiological or pathological conditions, might serve to modulate neuronal functions on one hand, or lead to degenerative processes on the other. (b) The neuropathic pain reported by patients who receive paclitaxel treatment [30] may result from the unexpected effects of paclitaxel on the MTs polar orientation. Namely, rather than "simply" stabilizing and condensing the MTs, long-term paclitaxel administration, induces MTs polar reconfiguration. This in-turn leads to different degrees of alterations in organelles transport (Fig. 7). The observed changes in MTs polar orientation do not recover after the withdrawal of the drug for up to 72 h suggesting that the newly formed MTs pattern is set to a new stable steady state (SS).

Reconfiguration of the MTs polar orientation in neurons

Two typical polar patterns of MT organization have been extensively documented in differentiated neurons. Axonal MTs have uniform orientation with their plus ends pointing towards the tip of the axons, whereas in dendrites MTs have mixed polar orientations (for review, [23]). Nevertheless, a number of studies documented that under experimental conditions the polar orientation of differentiated neurons can be altered [53, 60]. For example, in cultured *Aplysia* neurons, reversal of the MTs polar orientations was documented to occur within minutes of axotomy. In this case, massive MTs polar reconfiguration occurs in two steps: First, axotomy leads to a calcium dependent MTs depolymerization wave along the tip of the cut axon. This is followed by MTs repolymerization in a reversed polar orientation after the recovery of the calcium concentration [13, 20, 49, 63]. Stabilization of the retrograde orientation of the newly assembled MTs is attributed to molecular motors and organelles that accumulate at the site of MTs re-assembly [13]. The principles underlying

this mechanism were elegantly proposed and analyzed for the cases of MT reorientation in injured fragments of melanophores [8, 9]. Transformation of the typical uniform MTs orientation in axons, which is not preceded by an obvious depolymerization wave, occurs in cultured *Aplysia* axons as a consequence of expressing mutant human tau [49]. In the observations reported here, paclitaxel-induced MTs polar reorientation develops slowly over a period of 24–48 h. The process is not associated with elevation of the free intracellular calcium concentration or a massive wave of MT fragmentation.

Currently we do not know what mechanism underlies the paclitaxel-induced MTs polar reconfiguration. Based on the literature, a number of mechanisms could be considered: As demonstrated earlier, it is conceivable that intracellular paclitaxel generates new nucleation sites that sequester tubulin dimmers from which newly assembled MTs extend in various directions in the form of MTs asters [10, 18, 35]. It is also possible that paclitaxel interferes with molecular mechanisms that actively maintain the MTs pattern. For example, under normal conditions dynein propels plus end-distal MTs anterogradely into the axon [2], and moves minus end-distal MTs towards the soma excluding them from the neurite [12, 62], it is theoretically possible that paclitaxel interferes with yet unknown mechanism that maintain the pre-existing polar orientation of the MT population, leading to gradual change from the highly ordered MTs polar orientation to a chaotic SS.

An alternative theoretical explanation could be that paclitaxel induces existing dynamic MTs to loop and polymerize in the opposite direction and that since we imaged the dynamics of the MTs tips by EB3, we could not detect the formation of such hypothetical loops. Formation of MTs loops was observed within growth cones either spontaneously or following treatment with taxol [22, 31, 42, 56], while the contrary was reported by others [32]. It should be noted that whereas MTs "looping" was observed within GCs in which active linear polymerization of the MTs may have been impeded by the GCs plasma membrane. In the present study on the other hand, the change in MTs polar patterns took place within a preformed axonal structure in which the plasma membrane cannot impede the linear polymerization of MTs. It is important to note that imaging of SR101 labeled organelles retrograde transport along relatively long stretches of MTs never revealed the presence of "looping" pathways.

Based on the above arguments and observations, we suggest that in the presence of low paclitaxel concentrations new SS level vis a vis the polar orientations of the entire MT population is reached. The new SS is manifested by a significant shift in the polar orientations of MTs along the axon. Hence, whereas in a control neuron ~70% of the MTs orient their plus ends anterogradely, ~15% retrogradely and the rest (~15%) laterally, in 100 nM paclitaxel the proportions are altered such that ~46% of the MTs point anterogradely, ~32% retrogradely and ~22% laterally. As evidenced by the relationships between the equivalent vector of MTs polarity and organelle transport (Fig. 7), we propose that the impaired organelle transport is the outcome of the altered MTs polar orientation. Most likely, it is not due to direct competition of paclitaxel with molecular motors on MTs binding sites. This is based on studies which documented organelle transport along MTs stabilized by paclitaxel [48].

On the possible mechanisms that account for paclitaxel-induced peripheral neuropathy

Currently paclitaxel is extensively used as an anti-tumor drug [25]. Neurotoxicity of taxanes is the dose-limiting side effect for their use in clinics. A subset of patients receiving paclitaxel as chemotherapy for breast, ovarian and non-small cell lung cancers develop sensory peripheral neuropathy [1, 30, 36, 41]. While the use of paclitaxel in treatment of various tumors is increasing [40], methods to eliminate paclitaxel-induced peripheral neuropathy and sensory dysfunction are not available.

Studies aimed at understanding the source of taxane-induced peripheral neuropathy suggested a number of possible mechanisms: In vivo and in vitro exposure of chick and rat dorsal root ganglia neurons to 200 μM–10 mM paclitaxel (concentration that exceed the clinical dosage by over two orders of magnitude) revealed that paclitaxel inhibits anterograde and retrograde transport. This was attributed to the increased MTs density [54]. At concentrations of 1 μM–10 mM paclitaxel induces MTs condensation and abnormal distribution of the endoplasmic reticulum in dorsal root ganglia neurons [35, 54]. Taxane-induced axonopathy was reported to culminate in dying back of axons [16, 44, 47] or intraepidermal loss of sensory terminal arbors [50]. Consistent with these observations, we observed pathological features in the form of axonal swelling, blebbing of neurites, and detachment of axons from the substrate after paclitaxel application. Flatters and Bennet [17] proposed that paclitaxel-evoked neuropathic pain is due to toxic effects on mitochondria which lead to membrane depolarization and ectopic firing. Impaired organelle transport as reported here is expected to alter the maintenance of the neuronal functions and structures. Thus, impaired mitochondrial transport, protein turn-over and membrane cycling are expected to change the biophysical membrane properties, depolarize the membrane and lead to generation of ectopic firing [59]. We did not study in the present study the electrophysiology of neurons exposed to paclitaxel

for long periods and thus cannot corroborate these relations.

In addition, as described above, we found that the paclitaxel-induced MTs polar reorientation and transport defects are not reversible even after the removal of the drug for 3 days (Fig. 8). This is consistent with studies demonstrating that paclitaxel-induced peripheral neuropathy is only partially reversible upon termination of the treatment [6]. It has been demonstrated that paclitaxel concentration in cells is three orders of magnitude higher than the outside concentration, and that paclitaxel is retained in HeLa cells following washout for 24 h [26]. Thus, it would be conceivable that the recovery time of the axons may require long periods of wash. Nevertheless, we documented that within 24 h of paclitaxel washout the length of the EB3-GFP comet tails begins to recover suggesting that the intra axonal concentration of paclitaxel is effectively reduced. It is thus suggested that the new SS of the MTs population in combination with the distribution of the molecular motors and organelles is self-maintained for at least 3 days.

General implications

A comparison of human and *Aplysia* α and β -tubulin2 sequences resulted in 96–98% identities [49]. In vertebrates, paclitaxel was shown to compete with tau over MTs binding sites [27]. It is reasonable to assume that binding of paclitaxel to *Aplysia* MTs interferes with the association of *Aplysia*-tau in a similar manner to that reported for vertebrates. This is because *Aplysia* tubulin reveals a very strong similarity with human tubulin (96% identities, 99% positives for α-tubulin), and *Aplysia* MAP was found to contain three conserved MT binding repeats (E-values ranged between 1.9e-05 and 6.2e-12). Therefore, It is reasonable to assume that paclitaxel, which competes with tau over the MTs binding sites operates in *Aplysia* similarly to its operation in humans. In conclusion, the data presented in this study suggest that polar orientation of the MTs in differentiated neurons maintain the potential to be altered. Such alterations may serve physiological functions or lead to degeneration. In addition, our observations offer a mechanism that could account for the development of peripheral neuropathy in response to paclitaxel administration.

Acknowledgments This study was supported by the Israel Ministry of Health (300000-4955). Part of the work was done at the Charles E. Smith Family and Prof. Joel Elkes Laboratory for Psychobiology. The funders had no role in study design, data collection and analysis, decision to publish, or preparation of the manuscript. We thank Prof. Reuma Falk for statistical advice. Or Shemesh was partially supported by the Dimitris N. Chorafas foundation and by George Elias and Ada Tsur. M. E. Spira is the Levi DeViali Prof. in Neurobiology.

References

1. Argyriou AA, Koltzenburg M, Polychronopoulos P, Papapetropoulos S, Kalofonos HP (2008) Peripheral nerve damage associated with administration of taxanes in patients with cancer. Crit Rev Oncol Hematol 66:218–228
2. Baas PW, Black MM, Banker GA (1989) Changes in microtubule polarity orientation during the development of hippocampal neurons in culture. J Cell Biol 109:3085–3094
3. Baas PW, Karabay A, Qiang L (2005) Microtubules cut and run. Trends Cell Biol 15:518–524
4. Burton PR (1988) Dendrites of mitral cell neurons contain microtubules of opposite polarity. Brain Res 473:107–115
5. Burton PR, Paige JL (1981) Polarity of axoplasmic microtubules in the olfactory nerve of the frog. Proc Natl Acad Sci USA 78:3269–3273
6. Callizot N, Andriambeloson E, Glass J et al (2008) Interleukin-6 protects against paclitaxel, cisplatin and vincristine-induced neuropathies without impairing chemotherapeutic activity. Cancer Chemother Pharmacol 62:995–1007
7. Conde C, Caceres A (2009) Microtubule assembly, organization and dynamics in axons and dendrites. Nat Rev Neurosci 10:319–332
8. Cytrynbaum EN, Rodionov V, Mogilner A (2004) Computational model of dynein-dependent self-organization of microtubule asters. J Cell Sci 117:1381–1397
9. Cytrynbaum EN, Rodionov V, Mogilner A (2006) Nonlocal mechanism of self-organization and centering of microtubule asters. Bull Math Biol 68:1053–1072
10. De Brabander M, Geuens G, Nuydens R, Willebrords R, De Mey J (1981) Taxol induces the assembly of free microtubules in living cells and blocks the organizing capacity of the centrosomes and kinetochores. Proc Natl Acad Sci USA 78:5608–5612
11. De Vos KJ, Grierson AJ, Ackerley S, Miller CC (2008) Role of axonal transport in neurodegenerative diseases. Annu Rev Neurosci 31:151–173
12. Dehmelt L, Nalbant P, Steffen W, Halpain S (2006) A microtubule-based, dynein-dependent force induces local cell protrusions: implications for neurite initiation. Brain Cell Biol 35:39–56
13. Erez H, Malkinson G, Prager-Khoutorsky M et al (2007) Formation of microtubule-based traps controls the sorting and concentration of vesicles to restricted sites of regenerating neurons after axotomy. J Cell Biol 176:497–507
14. Erez H, Spira ME (2008) Local self-assembly mechanisms underlie the differential transformation of the proximal and distal cut axonal ends into functional and aberrant growth cones. J Comp Neurol 507:spc1
15. Falnikar A, Baas PW (2009) Critical roles for microtubules in axonal development and disease. Results Probl Cell Differ. doi: 10.1007/400_2009_2
16. Fazio R, Quattrini A, Bolognesi A et al (1999) Docetaxel neuropathy: a distal axonopathy. Acta Neuropathol 98:651–653
17. Flatters SJ, Bennett GJ (2006) Studies of peripheral sensory nerves in paclitaxel-induced painful peripheral neuropathy: evidence for mitochondrial dysfunction. Pain 122:245–257
18. Foss M, Wilcox BW, Alsop GB, Zhang D (2008) Taxol crystals can masquerade as stabilized microtubules. PLoS ONE 3:e1476
19. Galjart N (2005) CLIPs and CLASPs and cellular dynamics. Nat Rev Mol Cell Biol 6:487–498
20. Gitler D, Spira ME (1998) Real time imaging of calcium-induced localized proteolytic activity after axotomy and its relation to growth cone formation. Neuron 20:1123–1135
21. Hayashi K, Kawai-Hirai R, Ishikawa K, Takata K (2002) Reversal of neuronal polarity characterized by conversion of

dendrites into axons in neonatal rat cortical neurons in vitro. Neuroscience 110:7–17
22. Hendricks M, Jesuthasan S (2009) PHR regulates growth cone pausing at intermediate targets through microtubule disassembly. J Neurosci 29:6593–6598
23. Jaworski J, Hoogenraad CC, Akhmanova A (2008) Microtubule plus-end tracking proteins in differentiated mammalian cells. Int J Biochem Cell Biol 40:619–637
24. Jaworski J, Kapitein LC, Gouveia SM et al (2009) Dynamic microtubules regulate dendritic spine morphology and synaptic plasticity. Neuron 61:85–100
25. Jordan MA, Kamath K (2007) How do microtubule-targeted drugs work? An overview. Curr Cancer Drug Targets 7:730–742
26. Jordan MA, Wendell K, Gardiner S et al (1996) Mitotic block induced in HeLa cells by low concentrations of paclitaxel (Taxol) results in abnormal mitotic exit and apoptotic cell death. Cancer Res 56:816–825
27. Kar S, Fan J, Smith MJ, Goedert M, Amos LA (2003) Repeat motifs of tau bind to the insides of microtubules in the absence of taxol. Embo J 22:70–77
28. Kim T, Chang S (2006) Quantitative evaluation of the mode of microtubule transport in Xenopus neurons. Mol Cells 21:76–81
29. Komarova Y, De Groot CO, Grigoriev I et al (2009) Mammalian end binding proteins control persistent microtubule growth. J Cell Biol 184:691–706
30. Lee JJ, Swain SM (2006) Peripheral neuropathy induced by microtubule-stabilizing agents. J Clin Oncol 24:1633–1642
31. Letourneau PC, Ressler AH (1984) Inhibition of neurite initiation and growth by taxol. J Cell Biol 98:1355–1362
32. Lewcock JW, Genoud N, Lettieri K, Pfaff SL (2007) The ubiquitin ligase Phr1 regulates axon outgrowth through modulation of microtubule dynamics. Neuron 56:604–620
33. Lodish H, Berk A, Zipursky L et al (2000) Molecular cell biology, 4th edn. W. H. Freeman, New York
34. Ma Y, Shakiryanova D, Vardya I, Popov SV (2004) Quantitative analysis of microtubule transport in growing nerve processes. Curr Biol 14:725–730
35. Masurovsky EB, Peterson ER, Crain SM, Horwitz SB (1981) Microtubule arrays in taxol-treated mouse dorsal root ganglion–spinal cord cultures. Brain Res 217:392–398
36. Mielke S, Sparreboom A, Mross K (2006) Peripheral neuropathy: a persisting challenge in paclitaxel-based regimes. Eur J Cancer 42:24–30
37. Nakagawa H, Koyama K, Murata Y et al (2000) EB3, a novel member of the EB1 family preferentially expressed in the central nervous system, binds to a CNS-specific APC homologue. Oncogene 19:210–216
38. Nakata T, Yorifuji H (1999) Morphological evidence of the inhibitory effect of taxol on the fast axonal transport. Neurosci Res 35:113–122
39. Perez F, Diamantopoulos GS, Stalder R, Kreis TE (1999) CLIP-170 highlights growing microtubule ends in vivo. Cell 96:517–527
40. Pignata S, De Placido S, Biamonte R et al (2006) Residual neurotoxicity in ovarian cancer patients in clinical remission after first-line chemotherapy with carboplatin and paclitaxel: the Multicenter Italian Trial in Ovarian cancer (MITO-4) retrospective study. BMC Cancer 6:5
41. Postma TJ, Vermorken JB, Liefting AJ, Pinedo HM, Heimans JJ (1995) Paclitaxel-induced neuropathy. Ann Oncol 6:489–494
42. Rajnicek AM, Foubister LE, McCaig CD (2006) Growth cone steering by a physiological electric field requires dynamic microtubules, microfilaments and Rac-mediated filopodial asymmetry. J Cell Sci 119:1736–1745
43. Ruthel G, Hollenbeck PJ (2003) Response of mitochondrial traffic to axon determination and differential branch growth. J Neurosci 23:8618–8624
44. Sahenk Z, Barohn R, New P, Mendell JR (1994) Taxol neuropathy. Electrodiagnostic and sural nerve biopsy findings. Arch Neurol 51:726–729
45. Sahly I, Erez H, Khoutorsky A, Shapira E, Spira ME (2003) Effective expression of the green fluorescent fusion proteins in cultured Aplysia neurons. J Neurosci Methods 126:111–117
46. Sahly I, Khoutorsky A, Erez H, Prager-Khoutorsky M, Spira ME (2006) On-line confocal imaging of the events leading to structural dedifferentiation of an axonal segment into a growth cone after axotomy. J Comp Neurol 494:705–720
47. Scuteri A, Nicolini G, Miloso M et al (2006) Paclitaxel toxicity in post-mitotic dorsal root ganglion (DRG) cells. Anticancer Res 26:1065–1070
48. Seitz A, Kojima H, Oiwa K et al (2002) Single-molecule investigation of the interference between kinesin, tau and MAP2c. Embo J 21:4896–4905
49. Shemesh OA, Erez H, Ginzburg I, Spira ME (2008) Tau-induced traffic jams reflect organelles accumulation at points of microtubule polar mismatching. Traffic 9:458–471
50. Siau C, Xiao W, Bennett GJ (2006) Paclitaxel- and vincristine-evoked painful peripheral neuropathies: loss of epidermal innervation and activation of Langerhans cells. Exp Neurol 201:507–514
51. Spira ME, Dormann A, Ashery U et al (1996) Use of Aplysia neurons for the study of cellular alterations and the resealing of transected axons in vitro. J Neurosci Methods 69:91–102
52. Stepanova T, Slemmer J, Hoogenraad CC et al (2003) Visualization of microtubule growth in cultured neurons via the use of EB3-GFP (end-binding protein 3-green fluorescent protein). J Neurosci 23:2655–2664
53. Takahashi D, Yu W, Baas PW, Kawai-Hirai R, Hayashi K (2007) Rearrangement of microtubule polarity orientation during conversion of dendrites to axons in cultured pyramidal neurons. Cell Motil Cytoskeleton 64:347–359
54. Theiss C, Meller K (2000) Taxol impairs anterograde axonal transport of microinjected horseradish peroxidase in dorsal root ganglia neurons in vitro. Cell Tissue Res 299:213–224
55. Verstreken P, Ly CV, Venken KJ et al (2005) Synaptic mitochondria are critical for mobilization of reserve pool vesicles at Drosophila neuromuscular junctions. Neuron 47:365–378
56. Williamson T, Gordon-Weeks PR, Schachner M, Taylor J (1996) Microtubule reorganization is obligatory for growth cone turning. Proc Natl Acad Sci USA 93:15221–15226
57. Winer EP, Berry DA, Woolf S et al (2004) Failure of higher-dose paclitaxel to improve outcome in patients with metastatic breast cancer: cancer and leukemia group B trial 9342. J Clin Oncol 22:2061–2068
58. Xiao WH, Bennett GJ (2008) C-fiber spontaneous discharge evoked by chronic inflammation is suppressed by a long-term infusion of lidocaine yielding nanogram per milliliter plasma levels. Pain 137:218–228
59. Xiao WH, Bennett GJ (2008) Chemotherapy-evoked neuropathic pain: abnormal spontaneous discharge in A-fiber and C-fiber primary afferent neurons and its suppression by acetyl-L-carnitine. Pain 135:262–270
60. Yu W, Cook C, Sauter C et al (2000) Depletion of a microtubule-associated motor protein induces the loss of dendritic identity. J Neurosci 20:5782–5791
61. Zhang C, Sriratana A, Minamikawa T, Nagley P (1998) Photosensitisation properties of mitochondrially localised green fluorescent protein. Biochem Biophys Res Commun 242:390–395
62. Zheng Y, Wildonger J, Ye B et al (2008) Dynein is required for polarized dendritic transport and uniform microtubule orientation in axons. Nat Cell Biol 10:1172–1180
63. Ziv NE, Spira ME (1997) Localized and transient elevations of intracellular Ca2+ induce the dedifferentiation of axonal segments into growth cones. J Neurosci 17:3568–3579